JOURNAL OF SPACECRAFT AND ROCKETS
Vol. 47, No. 6, November–December 2010

Modeling and Experimental Validation of Space Structures with Wiring Harnesses

Vít Babuška*
Sandia National Laboratories, Albuquerque, New Mexico 87185
Douglas M. Coombs† and James C. Goodding‡
CSA Engineering, Albuquerque, New Mexico 87123
Emil V. Ardelean§
Schafer Corporation, Albuquerque, New Mexico 87106
and
Lawrence M. Robertson¶ and Steven A. Lane**
U. S. Air Force Research Laboratory, Kirtland Air Force Base, New Mexico 87117

DOI: 10.2514/1.48078

Power- and data-handling cables, which can account for up to 30% of a satellite's dry mass, couple with the spacecraft structure and impact dynamic response. Structural dynamic measurements suggest that a more complete representation of cable effects is needed to improve model predictive accuracy. To that end, a study was performed to characterize cable harness impacts on dynamic response. From this study, a finite element modeling method supported by empirically determined cable properties and structural behavior was developed. The modeling method was validated with a considerable amount of model simulation and experimental data for a variety of cables attached to a free–free beam. At low frequencies, the cable effect was dominated by mass and stiffness, changing the apparent stiffness; damping was a secondary effect. At higher frequencies, where the cables themselves were resonant, the cable effect was dissipative, increasing the apparent damping in addition to affecting the overall frequency response. Tiedown stiffness was found to be an important, but difficult to measure, parameter. Finite element models of a cabled beam were shown to be valid for all cable families studied. As a result, the finite element modeling method itself was validated.

Nomenclature

A	=	cross-sectional area, mm^2
d_C	=	cable diameter, mm
E	=	Young's modulus, MPa
EA	=	axial stiffness, N
EI	=	bending stiffness, Nm^2
E_β	=	accumulated root-mean-square response average error
f	=	frequency, Hz
$F_{\min}, F_{\max}$	=	frequency limits for root-mean-square response, Hz
f_A	=	axial force per unit length, N/m
f_T	=	transverse force per unit length, N/m
G	=	shear modulus, MPa
$G(f)$	=	frequency response function, mm/s/N
h_B	=	beam thickness, mm
h_{TC}	=	connector height, mm
I, I_{Eff}	=	area moment of inertia, mm^4
kG	=	shape factor shear modulus product, MPa
$K_1, \ldots, K_6$	=	Nastran generalized spring-and-damper structural element stiffnesses, N/m
k_{tie}	=	tiedown axial stiffness, N/m
k_X	=	axial spring stiffness, N/m
k_Z	=	transverse spring stiffness, N/m
k_θ	=	rotational spring stiffness, Nm/rad
L	=	cable length, mm
L_{RBE2}	=	Nastran rigid body element 2 length, mm
t	=	time, s
u	=	axial deflection, mm
v	=	transverse deflection, mm
x	=	position, $0 < x < L$, mm
x_0	=	boundary-condition position, mm
α	=	cross-section angle of rotation, rad
$\beta(f)$	=	accumulated root-mean-square response, mm/s
γ, γ_e	=	structural damping factors
ζ	=	modal damping ratio
ρ, ρ_{Cu}	=	mass density, kg/mm^3

Received 10 November 2009; revision received 9 July 2010; accepted for publication 25 July 2010.

*Principal Member of the Technical Staff. Associate Fellow AIAA.
†Associate Engineer. Senior Member AIAA.
‡Design Engineer. Senior Member AIAA.
§Research and Development Engineer. Senior Member AIAA.
¶Dynamics and Controls Program Manager, Space Vehicles Directorate. Associate Fellow AIAA.
**Senior Aerospace Engineer, Space Vehicles Directorate. Senior Member AIAA.

Introduction

THE evolution of precision spacecraft has led to structures of ever decreasing weight and specific mass, while the requirements on both static and dynamic mechanical stability have increased dramatically. For example, NASA's Origins science requirements lead to nanometer-level jitter stabilization requirements up to 1 kHz [1]. As a result, broadband structural control systems are being incorporated into space structures to meet mission and science goals. This levies additional requirements on structural dynamics models. In the early phases of a spacecraft program, structural control system concepts are developed based on preliminary structural dynamics models. Later, as component and subsystem designs evolve, the fidelity of structural dynamic and control models improve in step. Finally, structural dynamics models are validated, and input/output models for controller verification are identified during the final integration and test.

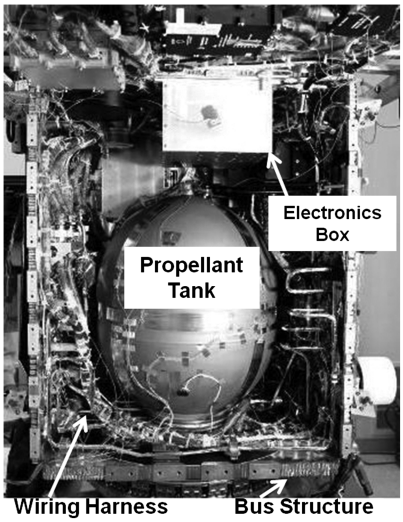

Fig. 1 AFRL spacecraft bus during final integration; note the many wrapped cable bundles.

Spacecraft require wiring harnesses for data and power transfers, which are often bundled together and attached to the payload structure. Figure 1 shows a U.S. Air Force Research Laboratory (AFRL) spacecraft during final integration. Although it was not a precision deployable spacecraft, the number of cables (and thus the mass) is significant and typical. Structural dynamic interaction of the cables with the host structure is usually not modeled. The contributions of wiring cables may be taken into account at the component level, for example, if a cable acts as load transmission path across a flexible interface or if the cable mass needs to be accounted for in a mass estimate.

At the spacecraft level, the influences of cable harnesses are first observed during system-level testing. For spacecraft for which the stowed and onorbit configurations are similar or do not have precision structural requirements, this is not a big problem; cable effects are localized. However, it may not be possible to ground test future deployable precision spacecraft to verify that onorbit performance requirements will be satisfied. Additionally, the bandwidth of structural control systems may be smaller than the jitter performance bandwidth, so precision space structures may have open-loop jitter requirements as well. Better knowledge of structural dynamic properties will be required at higher frequencies where dynamic interactions between cable harnesses and the host structure occur, and this knowledge will be needed earlier than the system-level test phase.

Background

It was difficult to find quantitative data on cable harness mass fractions in the open literature. The ESA Guidelines for Spacecraft Power and Signal Cabling [2] contain information from 15 small spacecraft that indicates mass fractions range from 4 to over 15%. Large spacecraft have more cables and can have mass fractions approaching 30%. While quantitative data are hard to find, qualitative information showing the significance of cable harnesses is available.

The majority of publications about cable dynamics deals with cables as primary structural elements [3] as, for example, in cable-stayed bridges. In the spacecraft area, Enberg describes the efforts of testing and the analysis of various candidate cables and umbilicals for microgravity science payloads on the International Space Station [4]. That work focused on the load transmissibility of the umbilical cables between an isolated microgravity experiment and the unisolated host structure. The effects of looping, large versus small displacements, and umbilical mounting configurations on the cable stiffness matrix were assessed. The NASA Jet Propulsion Laboratory Interferometry Program Experiment [1] included similar precautions to minimize stiffness coupling of sensor cables. Neither work made any effort to a priori model the interaction between the cables and the structure.

The contribution of instrumentation cables to damping has been observed in modal tests. For example, Griffith et al. [5] described modal tests of a wind turbine blade that were conducted with 96 accelerometers. When all but 12 were removed, the measured modal damping ratios decreased by up to 36% in the first three measured modes. The accelerometer cables did not affect the mode shapes, but their presence would have caused an overestimate of the damping that was greater than the measurement uncertainty.

From a dynamics and vibration attenuation perspective, continuous tuned-mass dampers have some commonality with the observed effects of cables on simple structures. Many references on continuous tuned-mass dampers can be found spanning more than 20 years. For example, Kitis et al. [6] described design methods for appending absorbers, including beams, to a host structure for reducing vibration response levels. While wiring harnesses have dissipative characteristics, vibration dissipation is not the primary design driver for a cable harness.

Early efforts at understanding the dynamic interaction between electrical cables and a host structure were performed at AFRL. These efforts used bundles of Teflon-coated wires attached to a truss structure, as shown in Fig. 2, and indicated that cable harnesses can shift modal frequencies and cause a significant increase in apparent damping, particularly in high-frequency modes. Figure 3 demonstrates the effect of adding four cable bundles (consisting of three cables per bundle) for a varying number of tiedown points. This illustrated that power and signal cable harnesses are a potentially critical component missed in the design and modeling of precision space structures.

Under the sponsorship of the AFRL Space Vehicles Directorate, a research effort was undertaken to understand the significance of cable harnesses on the structural dynamics of spacecraft, with a long-term goal of developing design tools for the structural dynamicist.

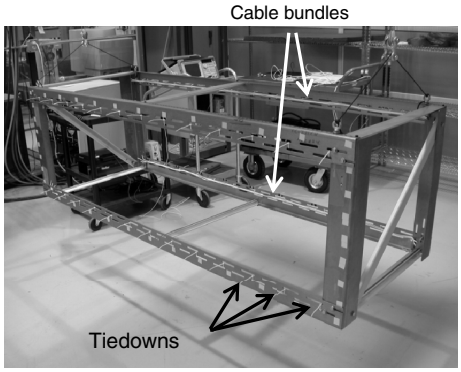

Fig. 2 Early cables and truss study setup.

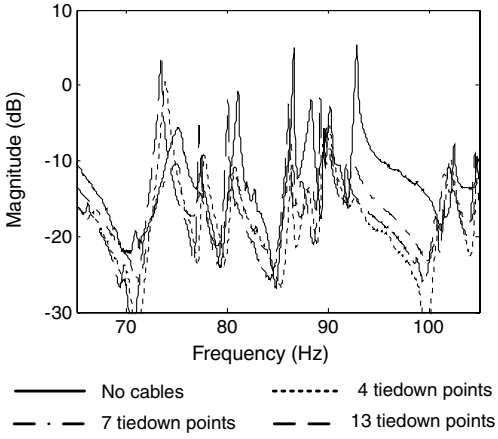

Fig. 3 Data demonstrating effect of cables and tiedowns on structural response.

Extensive efforts were dedicated to developing an understanding of intrinsic cable dynamics through cable-only testing and analysis [7–9]. Cable properties were derived from cable experiments, with the intent of creating a database of cable properties for use in modeling cabled structures. The study confined itself to Kapton-overwrapped stitched twisted-pair Teflon-coated wire cables.

In addition to the studies on cable harness dynamics, the interaction between cables and host structures was investigated. Cable-to-structure tiedown characteristics were studied experimentally and through model-based sensitivity analyses. The results from cable-only tests and tiedown studies were used to validate finite element models (FEMs) of cabled structures [10].

The free–free beam was selected as the host structure, because it is straightforward to model. It is also straightforward to measure its vibration response up to the frequency range in which cables are resonant. Having a validated cable-on-beam modeling approach is a prerequisite for modeling and analyzing the dynamic characteristics of more complex cabled structures, from spacecraft panels to complete satellites.

This paper describes the modeling and validation process for cabled structures using flightlike wiring cables on a free–free beam. First, linear finite element modeling of cables and their attachment to a host structure are reviewed. The study was confined to linear representations of wiring cables, because one objective was to evaluate how effectively standard, linear finite element analysis tools could be used for cabled structures. Next, the model validation philosophy is described. This section also includes a discussion of evaluation metrics used during model validation. The experimental configurations used are covered next, including the free–free beam test setup for rod-on-beam and cable-on-beam tests. Finally, with the cable and attachment properties and model forms in hand, the model validation of the cable-on-beam structure is described, including a discussion on various tiedown sensitivities. The paper concludes with a summary and interpretation of the main results.

Modeling Approach

Cable Representation

The objective of modeling a cabled structure is to understand the effects of the electrical cables on the dynamics of the host structure. There are two parts to the problem: modeling the cables themselves and modeling their attachment to the host structure. It was assumed that cables could be modeled as linear structures. The transverse vibration of harness cables can be represented by the equations of motion of shear beams [11] under the usual beam modeling assumptions (plane sections remain plane, etc.):

$$\rho A \frac{\partial^2 v(x,t)}{\partial t^2} + kGA\left(\frac{\partial^2 v(x,t)}{\partial x^2} - \frac{\partial \alpha(x,t)}{\partial x}\right) = f_T(x,t) \qquad (1)$$

$$\frac{\partial^2 \alpha(x,t)}{\partial x^2} + \frac{kGA}{EI}\left[\frac{\partial v(x,t)}{\partial x} - \alpha(x,t)\right] = 0 \qquad (2)$$

The shear modulus G, Young's modulus E, the cross-sectional area A, and the area moment of inertia I are considered to be independent parameters. By treating these four parameters as independent, G and E become effective quantities, not related by Poisson's ratio, and A and I are not tied to the physical cable diameter. The shear shape factor k is nominally 0.9 for a circular cross section. The axial vibration of a cable bundle is modeled using rod equations of motion[12]:

$$\rho A \frac{\partial^2 u(x,t)}{\partial t^2} + EA \frac{\partial^2 u(x,t)}{\partial x^2} = f_A(x,t) \qquad (3)$$

Torsion is ignored. Boundary conditions are applied at the tiedown points and at the ends where the cables attach to electronics boxes, as summarized in Table 1. Using these representations for transverse and axial vibration, a wiring harness cable can be modeled using standard Nastran beam or bar elements [13].

In addition to the mass and stiffness of the cables, their dissipative effects must be included in the model. Nastran provides four ways to introduce damping into a linear dynamics analysis model [13]: 1) overall structural damping with the Nastran parameter G (PARAM, G data card); 2) element structural damping GE specified on a Nastran material property definition bulk data card (MAT1); 3) modal damping through the Nastran modal damping definition bulk data card (TABDMP1); and 4) scalar viscous damping defined by the Nastran scalar damping element (CDAMP), the Nastran viscous damper element (CVISC), and the Nastran generalized spring-and-damper structural element (CBUSH) bulk data cards. The dissipative effects of the cables were captured by assigning an experimentally determined element structural damping factor γ_e to the cable bar elements on their MAT1 cards. This was the practical choice for segregating the damping contributed by the cables from the damping in the rest of the structure. Implicit in this choice is the assumption of constant modal damping in the cables. The magnitude of the frequency response functions (FRFs) at a modal frequency are equal when $\gamma = 2\zeta$, where γ is the modal damping factor. The differences in an FRF generated with structural damping rather than constant modal damping will be the greatest away from the modal frequencies where the response is small. An average modal damping factor was calculated for each cable type, so that when a structural damping factor is used, the FRF magnitudes would match those from the modal model of the cable at the resonant frequencies. A different approach is needed for a frequency-dependent damping representation. In summary, cables are modeled with bar or beam elements with six independent parameters: E, G, ρ, A, I, and γ_e.

Cable Attachment Representation

Cables are attached to host structures either directly with adhesive and/or tiedowns or to tabs, like those shown in Fig. 4. From a modeling perspective, attaching the cable to the host structure through tabs is preferable, because the interfaces are discrete. When tabs are used, the cable-to-host attachment can be modeled by connecting the cable elements to the host structure at discrete points, corresponding to the tiedown locations. In this configuration, the offset height as well as the stiffness and dissipation of the connection must be modeled. The offset height is important, because the axial stiffness of the cable couples into the bending stiffness of the host structure, since the neutral axes are not coincident. The stiffness of the connection is used to allow relative motion of the cable with respect to the host structure if the attachment is not perfectly rigid.

The Nastran rigid body element 2 (RBE2) and a six-degree-of-freedom (DOF) general spring element (CBUSH) are used for modeling the attachment in Nastran. The RBE2 length is given by

$$L_{\mathrm{RBE2}} = \frac{h_B}{2} + h_{TC} + \frac{d_C}{2} \qquad (4)$$

Table 1 Boundary-condition expressions

Clamped	Pinned	Free	Spring
$\alpha(x_0) = 0$	$\partial\alpha(x_0)/\partial x = 0$	$\partial\alpha(x_0)/\partial x = 0$	$(EI/L)[\partial\alpha(x_0)/\partial x] = k_\theta[\partial v(x_0)/\partial x]$
$v(x_0) = 0$	$v(x_0) = 0$	$\partial v(x_0)/\partial x = \alpha(x_0)$	$kGA[\partial v(x_0)/\partial x - \alpha(x_0)] = k_Z v(x_0)$
$u(x_0) = 0$	$u(x_0) = 0$	$\partial\alpha(x_0)/\partial x = 0$	$EA[\partial \mathrm{u}(x_0)/\partial \mathrm{x}] = k_X u(x_0)$

Fig. 4 TC-105 cable attachment hardware.

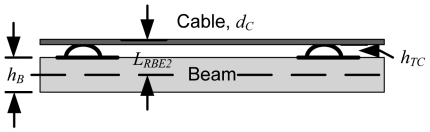

Fig. 5 L_{RBE2} length definition.

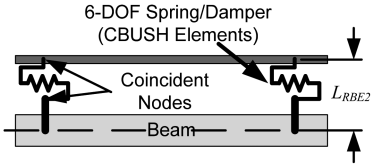

Fig. 6 CBUSH connectivity.

The parameters are illustrated in Fig. 5. For the TC-105 connector, shown in Fig. 4, $h_{\mathrm{TC}} = 4.76$ mm (3/16 in.). The master nodes are on the host structure, and the slave nodes are coincident with the appropriate cable nodes. In between the RBE2 nodes and the cable nodes, a CBUSH allows relative motion between the cable and the RBE2 (Fig. 6). The parameter values for the CBUSH card must be determined experimentally.

Cable Parameters

Spacecraft wiring harnesses include many types of cables. This study focused on only one type of cable: Kapton-overwrapped stitched, twisted pairs of Teflon-coated silver-plated copper wires (Fig. 7). The wires complied with MIL-W-22759/11 [14] specifications. Cables were fabricated according to industry best practice

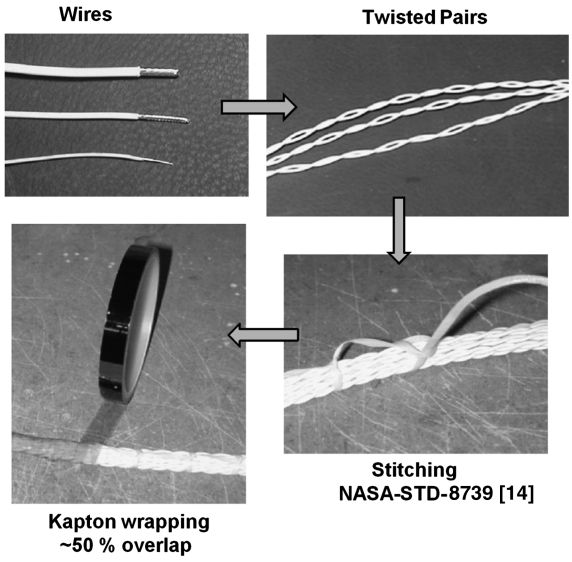

Fig. 7 Cable fabrication.

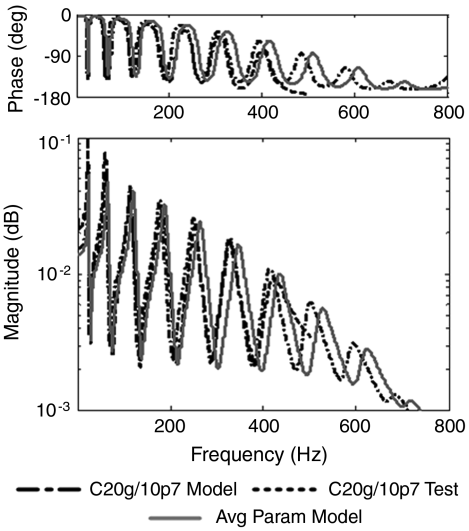

Fig. 8 Measured and model-generated FRFs for the 20g/10p7 cable specimen (model parameters: $E = 4 \times 10^5$ Pa, $kG = 1.124 \times 10^5$ Pa, $A_{\mathrm{Cu}} = 12.3$ mm^2, $I = 174$ mm^4, $\rho = 1.363 \times 10^{-5}$ kg/mm^3, and $\gamma = 0.06$).

and following NASA's STD-8739.4 for stitching, with differing numbers of twisted pairs as well as wires of varying gauges [15]. The nomenclature used to identify the cables is XXg/YYpZ, where XX refers to the wire gauge, YY refers to the number of twisted pairs, and Z identifies the sample; for example, sample 5 of a cable consisting of 30 twisted pairs of 26 gauge wire is denoted as 26g/30p5.

Cable stiffnesses were identified through axial and bending tests, as described by Goodding [16]. An average extensional modulus was calculated for each cable specimen family from the axial stiffness tests using the copper cross-sectional area. This average modulus and the copper cross-sectional area were used to identify the effective area moment of inertia I and the shear modulus G for each specimen sample from lateral vibration tests. A typical measured and Nastran-generated FRF is shown in Fig. 8. Only the cable bending response is observable in the FRF.

Since there was build-to-build variability between cable specimens, multiple samples were fabricated to create families and provide information on parameter variability. Tables 2–6 list the model properties and the amount of variability for the cables used in the study. As described by Goodding et al. [8] and Goodding [16], the cable parameters exhibited some specimen length dependence. The model parameters were derived from short cable specimens, usually 533 mm (21 in.) long. Short specimens were selected for two reasons: 1) many 533 mm cable specimens in each family were tested and 2) the node spacing with which the cable was attached to the host structure. The exception is the 26g/21p cable family. Four 26g/21p specimens (1, 2, 4, and 7) were available for cable-on-beam model validation, but the cable tests were performed with variable lengths, and specimens 1 and 2 were not stitched. No tests were performed on the unstitched specimens to establish their modulus, so the stitched modulus was used.

The cables were made by the same person in an attempt to minimize the human factor in build-to-build variability. Nevertheless, considerable variability exists in cable structural characteristics, as indicated by the variation in I_{Eff} and kG. The 20g/20p cables (Table 3) exhibited the greatest variability. The largest effective area moment of inertia is 4.4 times larger than the smallest. The 26g/21p cables were the most consistent. The frequency average ζ columns in Tables 2–5 show the modal damping factor averaged over all the identified modes of a specimen. As discussed previously, this average parameter was calculated so that cable element structural damping could be used. The variability over frequency was as high as two times larger than the specimen-to-specimen variability shown in the tables. The average parameters were used in the FEMs, as indicated by the values in the FEM parameters row.

Table 2 20g/10p cable properties[a]

Sample	Comment	Length, mm	Diam., mm	A_{Cu}, mm^2	ρ_{Cu}, kg/mm^3	E, MPa	I_{Eff}, mm^4	kG, Mpa	Freq. avg.ζ
20g/10p3		533.4	10.3	12.32	1.357E-05	4100	94.50	149.61	3.46%
20g/10p3	Test 1	635.0	9.8	12.32	1.331E-05	4100	274.79	61.48	4.47%
20g/10p3	Test 2	635.0	9.8	12.32	1.331E-05	4100	162.64	62.62	4.30%
20g/10p7		533.4	9.5	12.32	1.377E-05	4100	155.41	112.35	4.09%
20g/10p8		533.4	9.4	12.32	1.371E-05	4100	201.76	71.01	4.21%
20g/10p9		533.4	9.7	12.32	1.369E-05	4100	260.95	120.26	2.69%
20g/10p9	Family	533.4	9.7	12.32	1.375E-05	4100	219.55	107.45	3.87%
Average			9.733	12.32	1.363E-05	4100	195.7	97.8	3.87%
StDev[b]			0.35		1.734E-07		60.3	31.5	0.59%
COV			4%		1.27%		31%	32%	15%
FEM parameters		9.733	12.323	1.363E-05	4100	195.66	97.83	0.077	

[a]MAT1 structural damping parameter, $\gamma = 2\zeta$.
[b]Standard deviation.

Table 3 20g/20p cable properties[a]

Sample	Comment	Length, mm	Diam., mm	A_{Cu}, mm^2	ρ_{Cu}, kg/mm^3	E, MPa	I_{Eff}, mm^4	kG, Mpa	Freq. avg.ζ
20g/20p1	Test 1	533.4	14.0	24.65	1.314E-05	5000	274.89	79.04	3.66%
20g/20p1	Test 2	533.4	14.0	24.65	1.314E-05	5000	301.29	77.08	3.70%
20g/20p2	Test 1	533.4	14.5	24.65	1.362E-05	5000	312.60	124.49	3.46%
20g/20p2	Test 2	533.4	14.5	24.65	1.362E-05	5000	297.12	139.14	3.95%
206/20p3	Test1	533.4	14.5	24.65	1.364E-05	5000	269.79	91.28	4.27%
206/20p3	Test 2	533.4	14.5	24.65	1.364E-05	5000	256.70	132.80	3.23%
20g/20p4		533.4	14.4	24.65	1.315E-05	5000	312.55	107.61	2.99%
20g/20p6	Test 1	533.4	13.7	24.65	1.331E-05	5000	440.99	102.87	3.79%
20g/20p6	Test 2	533.4	13.7	24.65	1.331E-05	5000	1135.65	172.48	3.46%
20g/20p7		533.4	13.6	24.65	1.363E-05	5000	571.36	130.90	3.36%
20g/20p8		533.4	13.6	24.65	1.306E-05	5000	326.34	87.75	3.84%
20g/20p10		533.4	13.7	24.65	1.352E-05	5000	636.40	135.44	3.10%
20g/20pc	Family	533.4	13.6	24.65	1.348E-05	5000	679.04	134.49	3.54%
Average			13.957	24.65	1.339E-05	5000	450.83	117.84	3.61%
StDev			0.40		2.333E-07		243.91	27.52	0.36%
COV			2.9%		1.7%		54%	23%	10%
FEM parameters			13.957	24.646	1.339E-05	50	450.83	117.84	0.072

[a]MAT1 structural damping parameter, $\gamma = 2\zeta$.

Table 4 26g/10p cable properties[a]

Sample	Comment	Length, mm	Diam., mm	A_{Cu}, mm^2	ρ_{Cu}, kg/mm^3	E, MPa	I_{Eff}, mm^4	kG, Mpa	Freq. avg.ζ
26g/10p3		431.8	7.20	3.08	1.993E-05	10,500	15.76	137.53	2.72%
26g/10p6	Test 1	431.8	6.95	3.08	1.897E-05	10,500	11.67	146.91	4.12%
26g/10p6	Test 2	431.8	6.95	3.08	1.897E-05	10,500	11.55	199.06	3.30%
26g/10p7		431.8	7.00	3.08	1.923E-05	10,500	9.03	141.29	2.55%
26g/10p9	Test 1	431.8	6.80	3.08	1.930E-05	10,500	11.86	174.07	2.56%
26g/10p9	Test 2	431.8	6.80	3.08	1.930E-05	10,500	11.78	158.16	2.10%
Average			6.99	3.08	1.94E-05	10,500	11.94	159.50	2.89%
StDev			0.17		4.09E-07		2.16	23.46	0.71%
COV			2.4%		2.1%		18%	15%	25%
FEM parameters		6.988	3.081	1.936E-05	1050	11.94	159.50	0.058	

[a]MAT1 structural damping parameter, $\gamma = 2\zeta$.

Table 5 26g/21p cable properties[a]

Sample	Comment	Length, mm	Diam., mm	A_{Cu}, mm^2	ρ_{Cu}, kg/mm^3	E, MPa	I_{Eff}, mm^4	kG, Mpa	Freq. avg.ζ
26g/21p2	Not stitched	1143.0	9.00	6.47	1.798E-05	6500	107.94	242.50	4.87%
26g/21p2	Not stitched	533.4	9.00	6.47	1.798E-05	6500	108.05	220.44	1.76%
26g/21p4		889.0	9.20	6.47	1.830E-05	6500	102.31	118.69	4.42%
26g/21p4		533.4	9.20	6.47	1.830E-05	6500	92.97	212.54	2.72%
26g21p7		1041.4	9.00	6.47	1.813E-05	6500	81.30	170.75	3.41%
26g21p7		685.8	9.00	6.47	1.813E-05	6500	90.72	164.70	4.53%
26g21p7		381.0	9.00	6.47	1.813E-05	6500	84.14	168.99	3.65%
Average	w/o 26g/21p2		9.07	6.47	1.81E-05	6500	90.29	167.14	3.75%
StDev			0.12		1.64E-07		8.22	33.28	0.75%
COV			1.3%		0.9%		9%	20%	20%
FEM parameters			9.067	6.470	1.814E-05	6500	90.29	167.14	0.075

[a]MAT1 structural damping parameter, $\gamma = 2\zeta$. Stitched cable modulus used for 26g/21p2 unstitched cable.

Table 6 26g/30p cable properties

Sample	Comment	Length, mm	Diam., mm	A_{Cu}, mm^2	ρ_{Cu}, kg/mm^3	E, MPa	I_{Eff}, mm^4	kG, Mpa	Freq. avg.ζ
26g/30p1	Test 1	584.2	11.0	9.24	1.808E-05	6100	181.56	219.76	3.64%
26g/30p1	Test 2	584.2	11.0	9.24	1.808E-05	6100	170.37	211.47	2.37%
26g/30p1	Test 3	584.2	11.0	9.24	1.808E-05	6100	174.09	239.82	4.10%
26g/30p2		533.4	11.5	9.24	1.913E-05	6100	131.76	180.29	3.47%
26g/30p3		482.6	11.1	9.24	1.804E-05	6100	176.03	185.24	3.37%
26g/30p4		584.2	10.7	9.24	1.796E-05	6100	177.97	235.44	3.87%
26g/30p5		584.2	11.0	9.24	1.782E-05	6100	155.16	184.41	3.66%
26g/30p6		584.2	11.0	9.24	1.782E-05	6100	146.13	204.91	3.26%
26g30p7		584.2	11.1	9.24	1.800E-05	6100	135.95	153.81	3.71%
Average			11.06	9.24	1.81E-05	6100	161.00	201.69	3.49%
StDev			0.237		4.57E-07		19.15	28.16	0.49%
COV			2.1%		2.5%		12%	14%	14%
FEM parameters			11.057	9.242	1.812E-05	6100	1.690.070	201.69	0.070

Model Validation Philosophy

An objective in this work was to use the model validation process to validate the general cable modeling form rather than a specific model of a single system. Model validation is the process of determining how accurately a model represents the physical system for the intended use of the model. The validation process involves both model form and model parameters. If assumptions about, or constraints on, the model form yield unreasonable parameters to get a sufficiently accurate representation, then the modeling approach may be invalid. The modeling approach for cables and their attachment to a host structure was validated with a hierarchical approach, starting with tests of cables and tiedowns to determine their properties and using those parameters to create models of a cabled structure, as shown in Fig. 9. It is important to understand and minimize the errors in the identified parameters to avoid polluting the cabled structure model. To that end, the test configurations and parameter identification processes were validated by performing tests with reference specimens for which the properties were known.

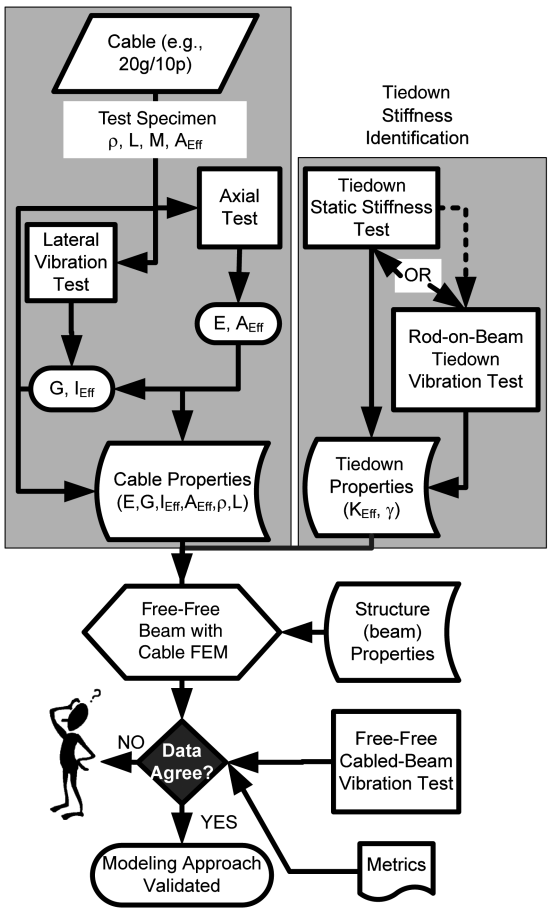

Fig. 9 Modeling approach validation process.

First, the FEM of the host structure was verified and validated. Since the host structure was a free–free beam, it was straightforward to model and tune to match experimental measurements. Next, cable properties were determined from both axial and lateral tests [8,16]. The tiedown stiffnesses were identified from two different tests: 1) a static stiffness test and 2) a test where rods, for which the properties were known, were attached to the host beam. The objective of the static test was to measure the tiedown stiffness directly. In the rod-on-beam configuration, the rod and beam properties were known, and the tiedown stiffness was the unknown determined by model-test correlation. Conceptually, the two tests could be hierarchical, where the rod-on-beam configuration serves as a validation experiment of the tiedown stiffness parameter determined from the static stiffness tests rather than an independent test for identifying the tiedown parameters.

With a valid model of the host structure, and an understanding of cable properties and parameters for attachment with the TC-105, models of the cabled beam were created. FRFs were computed with the models and compared with measured FRFs. If the data were in agreement for this set of structures, the modeling approach and parameters were deemed valid.

To understand and quantify the expectations on model accuracy and validity, models were created with both average cable family properties and cable specimen-specific properties (Tables 2–6). The first category of models corresponds to those in the design phases of a spacecraft program (Fig. 10), before specific as-built parameters are available. The cable parameters from individual cable specimens were used to create configuration-specific models. This category of models corresponds to later phases of a spacecraft development cycle. Finally, the models were used to evaluate different configurations, including variable tiedown spacing and cable placement.

Models were evaluated by quantitatively comparing model responses with test data using performance metrics. The metrics used depended on the type of test and modeling objectives. For the vibration tests, two correlation criteria were used: 1) resonance frequency error and 2) accumulated root-mean-square (rms) response, defined as

$$\beta(F) = \sqrt{\int_{\min}^{F} |G(f)|^2 \, \mathrm{d}f}, \qquad F_{\min} < F \leq F_{\max} \tag{5}$$

where the input is assumed to be unity magnitude white noise, so that $\beta(F)$ has units of response (e.g., mm/s). The correlation criteria are condensed to the maximum frequency error and the normalized average error in the accumulated rms response:

$$E_\beta = \frac{1}{n} \sum_{i=1}^{n} \frac{|\beta_{\text{meas}}(F_i) - \beta_{\text{FEM}}(F_i)|}{\beta_{\text{meas}}(F_i)} \tag{6}$$

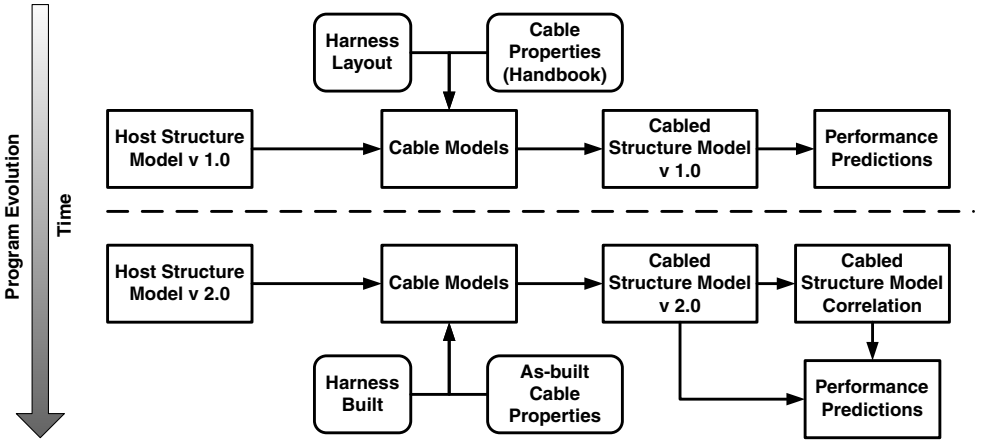

Fig. 10 Model evolution in spacecraft programs.

where $\beta_{\text{meas}}(F_i)$ is the accumulated rms response from $F_{\min}$ to F_i, and $F_n = F_{\max}$.

The criteria for parameter updating and model correlation are shown in Table 7. The maximum frequency error criterion is consistent with spacecraft modal testing criteria [17]. For the cable-on-beam validation tests, the objective was to quantify how well the models predict the cabled structure response, not to update model parameters. For these tests, the validation metrics were the same, but the criteria were relaxed, as summarized in Table 7.

Experimental Configurations

The cable and tiedown parameters used in the FEMs were determined independently by experimental tests. The cable properties were identified through cable-only testing [8,16], and the attachment CBUSH properties were determined by direct stiffness tests and rod-on-beam tests. The beam used to identify tiedown properties was also used for model validation of the cabled beam models.

Tiedown Stiffness: Direct Measurements

Estimates of the axial tiedown stiffness were obtained through direct measurements, with the test setup shown in Fig. 11. The shaker was attached to a stand so that the stinger and load cell were aligned with the specimen. The stinger was attached to the specimen with two-part epoxy and allowed to cure. Random excitation was applied with the shaker, and the response was measured with a laser vibrometer on the opposite end of the specimen. The shaker had a resonance at 10 Hz but, above this frequency, the response was flat to 200 Hz.

With this configuration, axial stiffness was obtained for different cable types, taking into account the zip-tie cable interface. A fundamental assumption in this test was that the deformation of the tiedown was consistent with the response of the cable and tiedown in the cabled structure. A quasi-static measurement would have been difficult to instrument, and a simple analysis of the connection suggested that a frequency dependence might exist because of the shaker dynamics. The test setup was designed considering the following factors:

1) The collocated frequency response measurement directly at the connection would have been virtually impossible to instrument.

2) Good alignment between the force transducer is easily achievable (to eliminate cross-axis loading); therefore, a flexible stinger and free–free boundary conditions for the shaker were not required. However, because the shaker base was not rigid, there was dynamic coupling between the shaker and the structure under test that had to be accounted for [18].

Table 7 Correlation and validation criteria

Metric	Correlation threshold	Validation threshold
Mode 1 frequency error	1%	3%
Max frequency error	5%	10%
Accumulated rms error, E_β	0.1	0.2

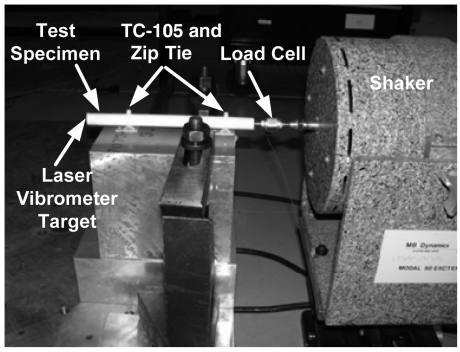

Fig. 11 Tiedown stiffness test configuration.

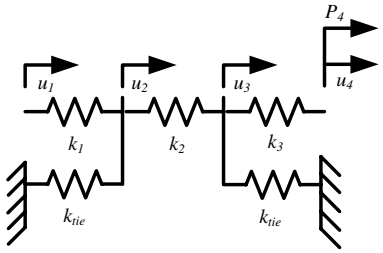

Fig. 12 Model representation of tiedown test configuration.

The test configuration was modeled as a series spring system, shown in Fig. 12, for which the equations of motion are

$$\{U\} = \{K\}^{-1}\{P\} = [C]\{P\} \tag{7}$$

where

$$K = \begin{bmatrix} k_1 & -k_1 & 0 & 0 \\ -k_1 & k_1 + k_2 + k_{\text{tie}} & -k_2 & 0 \\ 0 & -k_2 & k_3 + k_2 + k_{\text{tie}} & -k_3 \\ 0 & 0 & -k_3 & k_3 \end{bmatrix},$$

$$\{P\} = \{P_1 \quad P_2 \quad P_3 \quad P_4\}^T$$

and

$$\{U\} = \{u_1 \quad u_2 \quad u_3 \quad u_4\}^T$$

Since the test measured the $C_{1,4}$ term, $u_1/P_4 = C_{1,4}$, and the specimen stiffness was known, the tiedown stiffness k_{tie} was updated so that the $C_{1,4}$ term matched the measured compliance.

Rod-on-Beam Test Configuration

For the rod-on-beam tests, the validation host beam was suspended in a free–free configuration. Rod specimens 1270 mm (50 in.) long were attached every 101.6 mm (4 in.) along the centerline of the beam, with the TC-105 tabs and zip ties in the same configuration as the cables. Driving point FRF measurements were made using the shaker attached to the beam for excitation and the laser vibrometer sensor. Since the rod and beam properties were known a priori, the only unknown parameters were the tiedown stiffnesses. They were identified by correlating the FEM-generated FRF of the rod–beam structure with the measured FRF, using the metrics given in Eqs. (5) and (6) and the criteria listed in Table 7. The fundamental assumption in this approach is that the zip-tie rod interface is sufficiently equivalent to the zip-tie cable interface. The advantage is that the attachment is exercised as it is in the cabled structure. In principle, all six stiffness terms can be identified; however, since the rod was centered on the beam, and the beam was only excited in one axis, only three terms were identified.

Validation Beam Structure

The host structure for all rod-on-beam and cable-on-beam experiments was a 1270 mm (50 in.) free–free beam (Fig. 13) with a uniform cross-section of 12.7×50.8 mm (0.5×2 in.). A relatively simple structure for which the parameters could be accurately identified was important so that uncertainty from the host structure did not obscure the effects of the cables and their attachments in the measured data. The beam was designed to have the first bending mode at 40 Hz, which is realistic for space structures as well as providing an easily measured dynamic stiffness line.

The beam was suspended with long bungee cords to simulate free–free boundary conditions. An electromagnetic voice-coil shaker provided the input force. A load cell was rigidly connected to the beam to measure the force transmitted from the shaker through a stinger. A laser vibrometer measured the velocity of the beam at the driving point. Continuous and burst random signals were generated to excite the structure, and a Hanning window was used with the continuous random signal to reduce leakage. The maximum frequency bandwidth for the experiments was 1 to 2000 Hz.

Results

Validation Beam Model

The validation free–free beam was modeled carefully in Nastran using plate (CQUAD4) elements, so that modeling effects of the host structure would not obscure the cable effects. Driving point measurements were made at two locations: 140 mm (5.5 in.) or 216 mm (8.5 in.) from the end of the beam. The modulus E was updated to correlate the model with the measured driving point FRF,

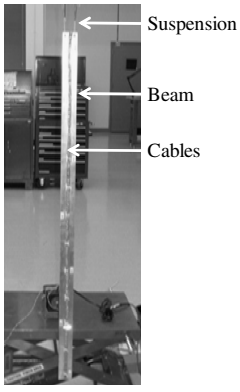

Fig. 13 Free–free beam test structure.

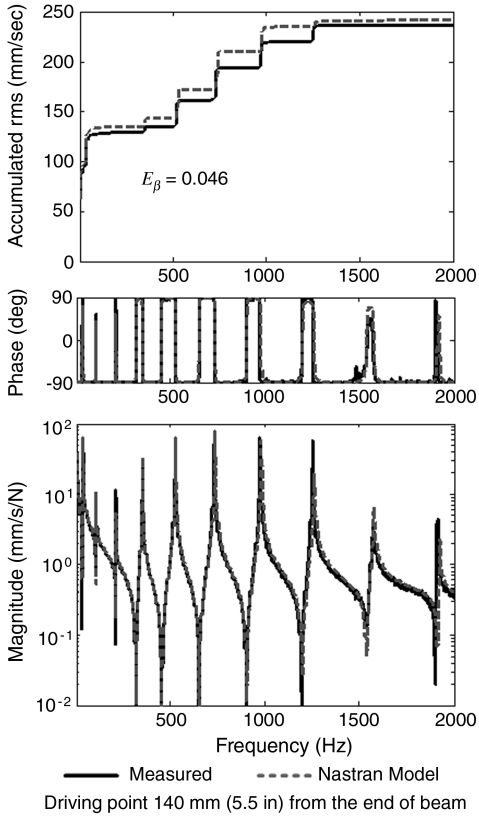

Fig. 14 Measured and Nastran-generated FRFs and accumulated rms error for host structure.

shown in Fig. 14, using the two metrics described previously. The model-generated FRF used the same frequency points as the test to minimize differences caused by discretization of the FRF. Frequency-dependent modal damping was applied with the TABDMP1 card. The damping levels were estimated from an identified model of the beam. The measured rms response was computed from the FRF rather than from a time history. The error in the accumulated rms response, Eq. (5), was 5.6% through 800 Hz and 4.5% through 2000 Hz, as illustrated in Fig. 14, because damping was undermodeled for some modes.

Cable Attachment Properties

The axial tiedown stiffnesses determined from the direct measurements on the aluminum, copper, and polytetrafluoroethylene

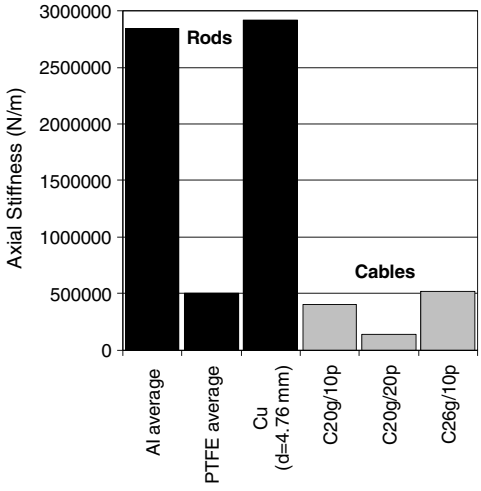

Fig. 15 Direct measurement tiedown stiffness.

Table 8 Rod properties

Rod material	Copper alloy	Copper alloy	T-6061 aluminum	T-6061 aluminum	PTFE
d_C [a], mm	4.76	4.0	4.76	9.53	9.53
No. of specimens	1	2	3	2	1
Avg E [a], GPa	116.3	119.9	67.76	62.64	1.478
COV, %	N/A	6.08	2.25	4.72	N/A
ρ [b], kg/mm^3	8.913×10^{-6}	8.913×10^{-6}	2.723×10^{-6}	2.723×10^{-6}	2.242×10^{-6}
L [a], mm	584.2	584.2, 1092.2	584.2, 1092.2	584.2, 1092.2	584.2
Avg. EI, N·mm^2	2.936×10^6	1.469×10^6	1.711×10^6	2.478×10^7	0.5846×10^6
Avg. EA, N	2.071×10^6	1.483×10^6	1.207×10^6	4.464×10^6	0.1053×10^6
γ_e	0	0	0	0	0.02

[a]Measured.
[b]Handbook value.

Table 9 Rod-on-beam model correlation summary

Property	Beam with copper rod		Beam with aluminum rod		Beam with PTFE rod	Bare beam
d_C, mm	4.76	4.0	4.76	9.53	9.53	——
Bandwidth, Hz	800	2000	2000	2000	800	800
Mode 1 error		2%			1%	0%
Max. freq. error	3.0% at 729 Hz	4.1% at 804 Hz [a]	3.9% at 1264 Hz	3.8% at 1843 Hz [a]	2.4% at 728 Hz	0.6% at 352 Hz
E_β	0.075	0.041	0.064	0.035	0.19	0.13

[a]Model FRF did not show all cable modes. Driving point 216 mm (8.5 in) from end of beam.

(PTFE) rods are summarized in Fig. 15. Axial tiedown stiffness was also estimated from measurements made with three cable specimens. A single tiedown configuration (i.e., a short segment with only one TC-105 tiedown rather than the two shown in Fig. 11) was used for these tests. The tiedown stiffnesses were $\frac{1}{3}$ to an order of magnitude lower than those extracted from rod-on-beam tests that are subsequently described.

The same three rods were used for the rod-on-beam tests to estimate the tiedown parameters. The specimen properties, shown in Table 8, were extracted from the driving point, transverse vibration FRFs of 584.2 mm (23 in.) and 1092.2 mm (43 in.) clamped–clamped rod specimens. The measured modal frequencies and Bernoulli–Euler beam theory [12] agreed to better than 1% in the first five modes in each test.

The individual rod specimens were attached to the beam every 101.6 mm (4 in.) along the centerline of the beam. Driving point FRF measurements were made, and the CBUSH parameters that modeled the tiedown stiffnesses and structural damping were updated to correlate the FEM with the measured FRFs. The driving point was located 216 mm (8.5 in.) from the end of the beam. The torsion DOF (rotation about the x axis) was constrained in the model. The tiedown stiffness properties were estimated by minimizing the resonance frequency error and the accumulated FRF rms error. The minimization was performed manually rather than with a formal parameter optimization such as Nastran SOL200.

Good correlations between Nastran-generated FRFs and the measured FRFs for all five rod-on-beam configurations were obtained by selecting $K_1 = K_2 = K_3 = 5.25 \times 10^6$ N/m (3×10^4 lb/in.) and $K_5 = K_6 = 11.3$ N·m/rad (100 in.·lb/rad) for the CBUSH stiffness entries. As the excitation and responses were exclusively in bending, the models were insensitive to the lateral stiffness K_2 and the rotational stiffness K_6, so these values effectively were arbitrary for this configuration. The vertical tiedown stiffness K_3 was set equal to K_1 for convenience. If K_3 was too low, local cable modes were observable in the model-generated FRFs. The 9.53 mm (3/8 in.) Al beam-on-rod model correlation was improved by 2% at low frequencies using $K_1 = K_2 = K_3 = 7.01 \times 10^6$ N/m (4×10^4 lb/in.) and $K_5 = K_6 = 11.3$ N·m/rad (100 in.·lb/rad). The CBUSH damping parameters were rod dependent. For the PTFE and 4.76 mm (3/16 in.) Cu rods, $GE_1 = GE_2 = GE_5 = GE_6 = 0.1$ worked well. For the others, setting GE_1–GE_6 to zero gave the best cumulative rms correlation. The results are summarized in Table 9. While the frequency errors of the rod-on-beam models were larger than the model of the bare beam, they were less than 5%, which was deemed acceptable. The accumulated rms error E_β was sensitive to the damping levels in the model.

The PTFE rod was most like a cable. The PTFE rod-on-beam model captured the mode splitting and rod–structure interaction at 476 and 576 Hz, as illustrated in Fig. 16. It overestimated the

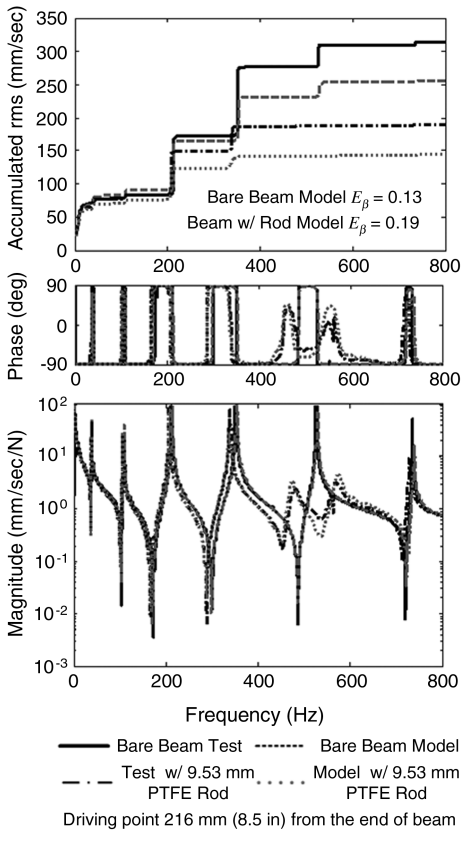

Fig. 16 PTFE rod-on-beam FRFs and accumulated rms response.

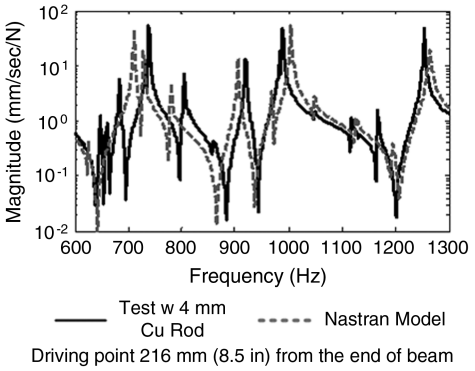

Fig. 17 4 mm Cu rod-on-beam FRFs and accumulated rms response ($E_\beta = 0.041$).

damping in the 202 Hz mode, which is reflected in the relatively large value of E_β in Table 9. This was not a function of the tiedown parameters; it was a function of the element structural damping used to model the rod. Figure 16 also displays the FRFs of the uncabled beam and its Nastran model, clearly showing the effects of the PTFE rod on the transverse vibration response. Note that Figs. 14 and 16 are different, because they show different driving point measurements. The bare beam model TABDMP parameters were optimized on the low-frequency modes of the 140 mm driving point, shown in Fig. 14. The PTFE rod–beam combination showed the most sensitivity to the K_5 and K_6 CBUSH parameters. The frequency of the resonance peak at 476 Hz was underpredicted with $K_5 = K_6 = 0$ and was well correlated with $K_5 = K_6 = 11.3$ N·m/rad (100 in.·lb/rad).

Figure 17 shows model and measured FRFs of the 4 mm copper rod-on-beam test case zoomed in on 300–600 Hz. The driving point was 216 mm (8.5 in.) from the end of the beam. This copper rod-on-beam case showed the poorest correlation, because not all of the modes visible in the measured FRF are represented in the Nastran model FRF.

The tiedown stiffness values determined from the direct measurements were used in the rod-on-beam Nastran models to evaluate the validity of the direct tiedown stiffness measurements. The translational stiffnesses were set to the values shown in Fig. 15. The 11.3 N·m/rad value was used for the rotational stiffnesses. The model-generated FRFs are compared with measured FRFs in Figs. 18 and 19. These figures show that the tiedown stiffnesses obtained from the direct measurements of the rods were too low when

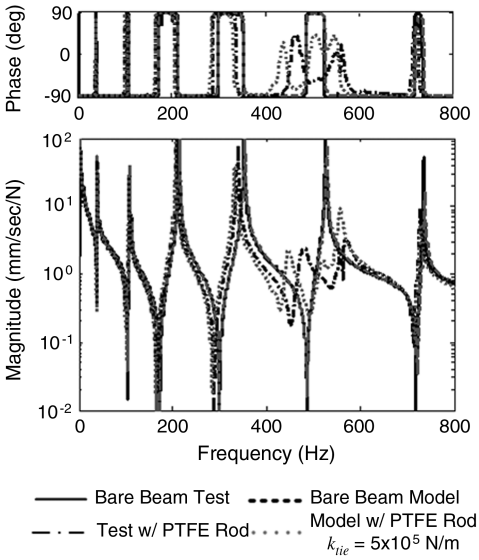

Fig. 18 PTFE rod-on-beam FRF with tiedown stiffness from direct measurement.

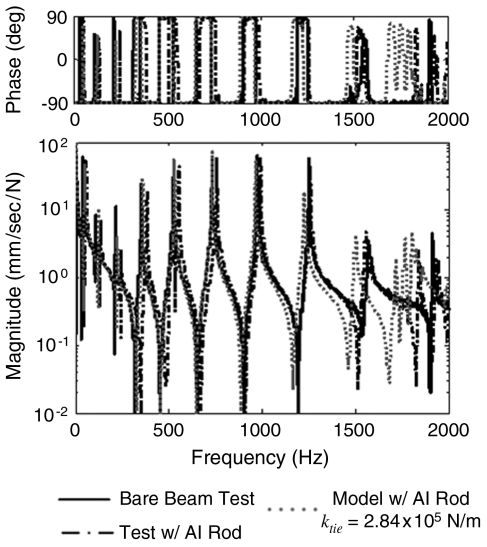

Fig. 19 9.5 mm Al rod-on-beam FRF with tiedown stiffness from direct measurement.

applied to the rod-on-beam configurations. For example, the low-frequency modes were underpredicted with these tiedown stiffnesses. As a result, the stiffnesses obtained from the direct measurement tests were not used. Based on the tiedown stiffness study, CBUSH stiffness parameters $K_1 = K_2 = 5.25 \times 10^6$ N/m (3×10^4 lb/in.) and $K_4 = K_5 = 11.3$ N·m/rad (100 in.·lb/rad) were used to represent the cable tiedown stiffness.

L_{RBE2} Sensitivity

Before moving on to the cable-on-beam configurations, the sensitivity of the rod-on-beam interaction to L_{RBE2} length was evaluated using the 9.53 mm ($\frac{3}{8}$ in.) Al and PTFE rod-on-beam configurations. These two configurations were selected because they represented the extremes of rod axial stiffnesses (see Table 8). The L_{RBE2} length in the models was varied from 0 to 19 mm (0.75 in.). The tiedown stiffnesses were the best values determined from the tests described previously. When $L_{\mathrm{RBE2}} = 0$, the rod and beam neutral axes are coincident, and there is no coupling between the axial stiffness of the rod and the bending stiffness of the beam. The PTFE rod-on-beam configuration showed little sensitivity to L_{RBE2} length. The aluminum rod-on-beam FRF in Fig. 20 shows the importance of L_{RBE2} length for stiff rods/cables. The geometrically correct value for a particular cable, given by Eq. (3), should be used, but approximating it may not be a felonious modeling crime, particularly for compliant cables.

Cable-on-Beam Results

Four cable families, 20g/10p, 20g/20p, 26g/10p, and 26g/30p, were tested on the free–free beam. The cables were attached to the

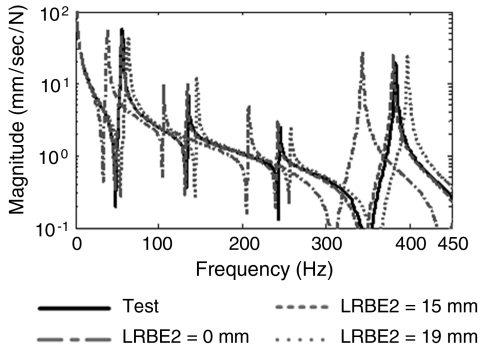

Fig. 20 L_{RBE2} effects on 9.7 mm Al rod-on-beam FRF.

Table 10 Cable-on-beam model correlation summary

	20g/10p, 9%[a]		20g/20p, 18%[a]			26g/10p, 3%[a]	26g/21p, 6%[a]	26g/30p, 9%[a]
Parameter source	Average	20g/10p3	Average	20g/20p1 (best fit)	20g/20p7 (worst fit)	Average	Average	Average
Bandwidth, Hz	2000	2000	800	800	800	800	800	800
Mode 1 error	6%	4.1%	4%	1.6%	4%	1%	3%	1%
Max. freq. error	6% at 41 Hz	4% at 41 Hz [b]	4% at 453 Hz	5% at 770 Hz [b]	9% at 453 Hz	3% at 750 Hz	3% at 40 Hz	7% at 408 Hz
E_β	0.076	0.09	0.14	0.015	0.21	0.18	0.12	0.18

[a]Cable mass ratio (1270 mm cable).
[b]Driving point 216 mm (4.5 in) from end of beam.

centerline of the beam every 101.6 mm (4 in.) with the TC-105 tabs, as illustrated in Fig. 13. The driving point was 216 mm (4.5 in.) from the end of the beam. Cable properties were obtained from cable-only tests described previously. The results for all four families are summarized in Table 10 and discussed in detail in the following sections. The cable-on-beam data had different frequency spacings, so all FRFs were interpolated to appropriate frequency lines to ensure a valid comparison of accumulated rms levels and errors.

Cable Family 20g/10p

Figure 21 shows the results from the 20g/10p family. Only two cable specimens from this family, 20g/10p3 and 20g/10p5, were tested attached to the host structure. Both the average parameter model and the specimen-specific model correlate well with the measured data. The maximum frequency errors were 6 and 4.1%, and the accumulated rms errors were 0.076 and 0.09 for the average parameter model and the specimen-specific model, respectively. The first mode frequency error was between 4 and 6%, which is well within the validation threshold in Table 7. The 20g/10p cable-on-beam model was slightly stiff (39 vs 41 Hz) in the low-frequency range. For this family, the difference between the average property model and the specimen-specific model was small overall; in fact, the specimen-specific model underestimates the damping as evidenced by the slightly larger E_β metric. Both the average parameter and specimen-specific models overestimate the response at 781 Hz, showing a mode that is not as observable in the test FRF. Similarly, the models underestimate the effective damping in the 1900 Hz mode, but the specimen-specific model is slightly better. This shows the sensitivity of the response to cable properties.

One of the difficult cable parameters to identify was the shear modulus G because of the small slenderness ratios of the cables [16]. Figure 22 suggests that the effort was not in vain. The figure compares FRFs generated using a Bernoulli–Euler beam assumption for the cable with the shear beam cable model and with measured FRFs. Both models compared well with the measured FRFs in the first three modes, before the cable and host–beam interaction frequency range. The Bernoulli–Euler model did not capture the cable–beam interaction correctly, specifically around 400 and 750 Hz, clearly showing the Bernoulli–Euler assumption inadequate, at least for the 20g/10p family.

Cable Family 20g/20p

The 20g/20p family was the largest family tested, consisting of nine specimens, of which four were tested on the host structure. Test FRFs and a model-generated FRF using family average parameters are compared in Fig. 23. The figure shows the effects of cable parameter variations. Below 200 Hz, the cable effects were consistent and very well represented by the model. Above 200 Hz, the FRF similarity is reduced. The cables had a large effect on the response level; resonance peak amplitudes were reduced by an order of magnitude, which the model captured. The model seems to be too stiff in the main beam–cable interaction frequency band, 250–450 Hz. Because of the large variance in the effective area moment of inertia, the accuracy of the average parameter model was limited. Nevertheless, Fig. 23 shows that the average parameter model was representative of this cable family's effects on the host structure.

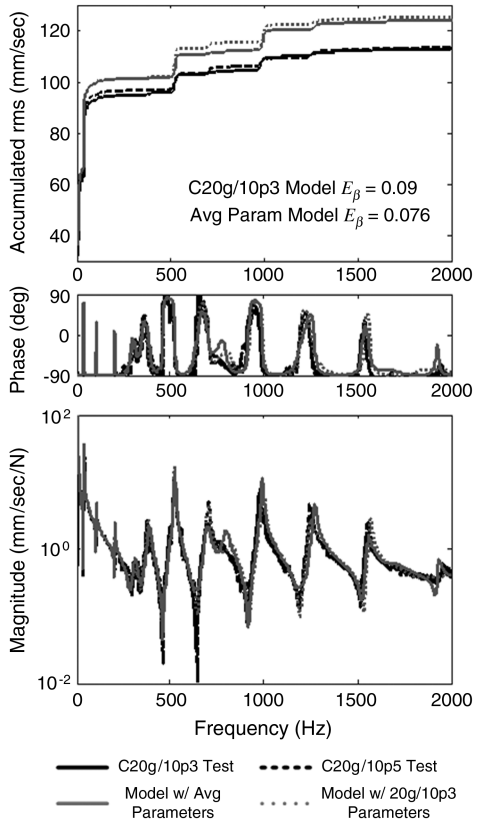

Fig. 21 20g/10p Model and test FRF and accumulated rms error comparison.

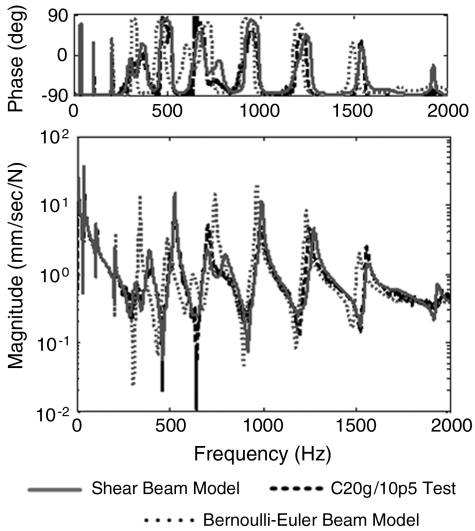

Fig. 22 Comparison of BE and shear beam model assumptions for 20g/10p cable on beam.

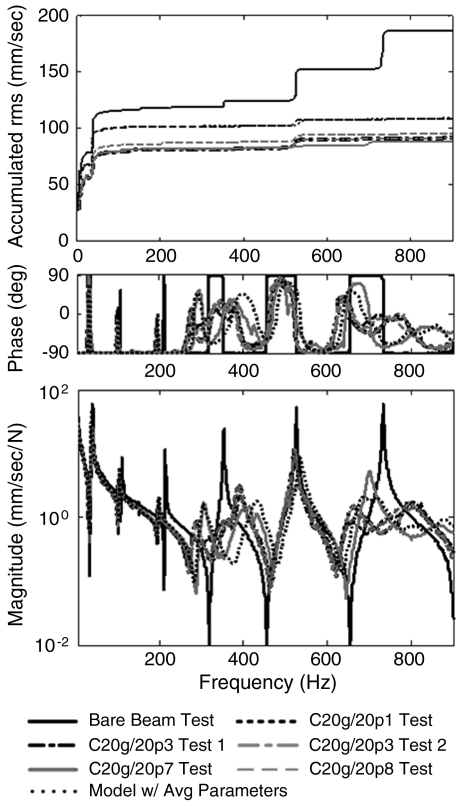

Fig. 23 20g/20p cable-on-beam comparison: test and average parameter model.

Figure 24 shows the modeled and measured FRFs for cable 20g/20p1 on the host structure. The figure shows that both the average parameter model and the specimen-specific model accurately fit the modes below 200 Hz. The specimen-specific model captures the cable–beam interaction in the 250–450 Hz band better than the average parameter model. Both models underestimated the modal frequency and damping ratio of the 800 Hz mode. The accumulated rms error of the average parameter model is better than the specimen-specific model, because the 800 Hz mode is underdamped in the specimen-specific model. This example shows the benefits of using specimen-specific parameters as they become available (Fig. 10).

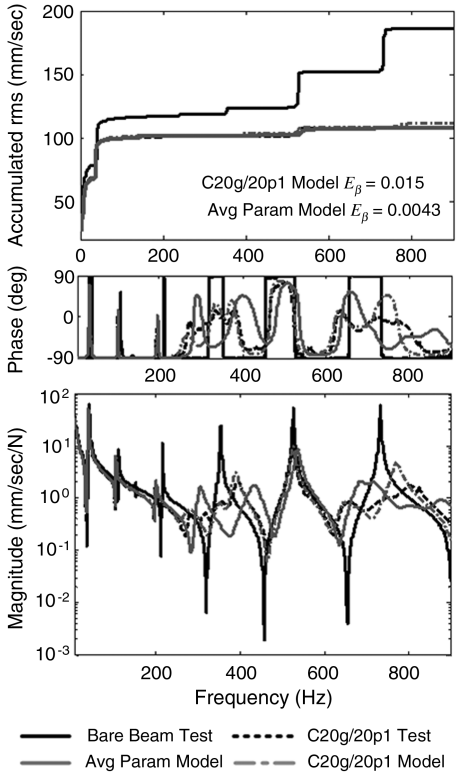

Fig. 24 20g/20p1 model and test FRF and accumulated rms error comparison.

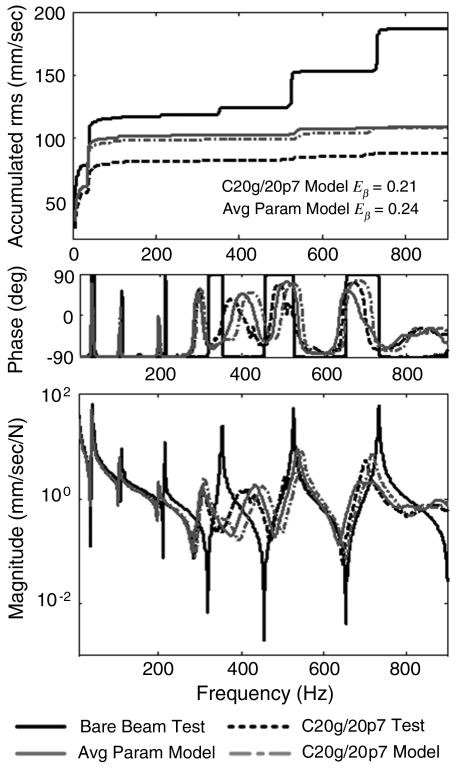

Fig. 25 20g/20p7 model and test FRF and accumulated rms error comparison.

On the other hand, Fig. 25 shows a case where the specimen-specific model is not clearly better than the average parameter model. Specimen 20g/20p7 interacts with the host structure differently than the other specimens, as can be seen in Fig. 25. While 20g/20p1 was more compliant than the average cable (i.e., I and kG are smaller than the average values), specimen 20g/20p7 was stiffer: note the relative positions of the modal peaks in Fig. 25. While the 20g/20p7 model is too stiff, the accumulated rms error is lower. In this case, the specimen-specific cable parameters did not lead to an obvious improved model, and neither the average model nor the specimen-specific model satisfies the validation criteria.

Specimen 20g/20p2 was cut into 330 mm (13 in.) segments that were attached to the host beam, as illustrated in Fig. 26. Figure 27 shows that the model of this configuration is a reasonable representation; it adequately predicts the cable–beam interaction between 250 and 900 Hz. It underpredicted the damping in modes 1, 2, and 8 and overpredicted the damping in the last two modes. The large response in the first mode was the main contributor to the rms error metric, which at $E_\beta = 0.18$ shows that the model satisfies this validation criterion. This figure shows that the cable-on-beam models can predict the dynamics of short cables on the host beam.

Cable Family 26g/10p

Cable-on-beam experiments were also conducted with thinner 26 gauge wire. A 1270 mm (50 in.) 26g/10p cable is very light, weighing in at only 3% of the host beam. The presence of the cable had only a small impact on the host structure response, as shown in Fig. 28. Three specimens were tested on the host beam, and the variation in the measured FRFs was small compared with the variation observed for other cable families. This was due to the

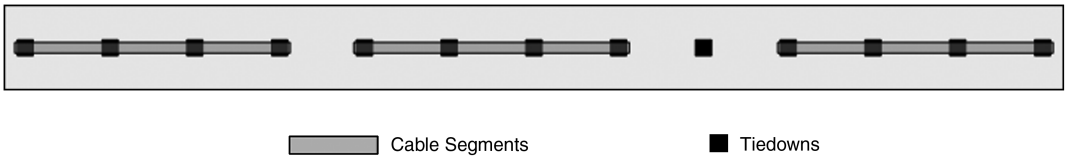

Fig. 26 Three-segment cable-on-beam configuration.

similarity of the cables, as indicated by the relatively small coefficient of variation (COV) (Table 4) and their light weight. The main effect was an increase in the apparent damping, which the model generally underpredicts. Nevertheless, the model satisfies the validation criteria, confirming its adequacy. This effect is consistent with observations made in modal tests (e.g., [5]) regarding the effects of instrumentation cables, which by design are a small fraction of the test article's mass.

Cable Family 26g/21p

The 26g/21p cable had a noticeably larger effect on the host beam than the 26g/10p cable, as illustrated in Fig. 29. For this cable family, the cable parameters did not exhibit a strong sensitivity to cable length, and the average cable properties were calculated over all cables. The primary cable–structure dynamic interaction was between 300 and 450 Hz. The average parameter model predicted this interaction well. The overall response level was also well represented by the model, with a 12% accumulated rms error. Since the validation criteria are satisfied, the model can adequately represent the response of the beam with the 26g/21p cable attached.

Early in the research program, a few unstitched cables were fabricated and tested before the cable fabrication was standardized to include stitching. Two nominally identical 26g/21 specimens were fabricated without stitching. One was used for cable property tests; the other was used in cable-on-beam tests. The damping estimated in the cable test was low and, surprisingly, the specimens were stiffer than average. Figure 30 shows the measured and model-generated FRFs as well as the accumulated rms response. The low damping in the specimen model leads to an E_β that is outside the validation threshold. The average parameter model damping estimate was higher and, as a result, this model did satisfy the validation criteria. Figure 30 and Table 5 suggest that stitching may reduce the cable stiffness, or its impact is smaller than the cable build-to-build variability. The notion that unstitched cables are stiffer than stitched cables is counterintuitive, so the data suggest that stitching is not significant to cable stiffness. Since it is always risky to draw inferences from a single data set, more investigation into fabrication influences on cable properties is required.

Cable Family 26g/30p

The mass fraction of the 26g/30p cable is comparable to the 20g/10p cable, and the effects on the response of the host beam were qualitatively similar. Figure 31 shows the model-generated and test FRFs up to 800 Hz and the corresponding accumulated rms error. The bare beam is included for reference. The splitting of the fourth mode was captured by the model, which was stiff in this region, since the frequency of mode 5 is 7% too high. The damping in the cabled structure model also was slightly low, particularly in the low-frequency region. After the first mode, the model does a good job predicting the response level. The validation criteria are satisfied, indicating that the model can adequately represent the response of the beam with the 26g/30p cable.

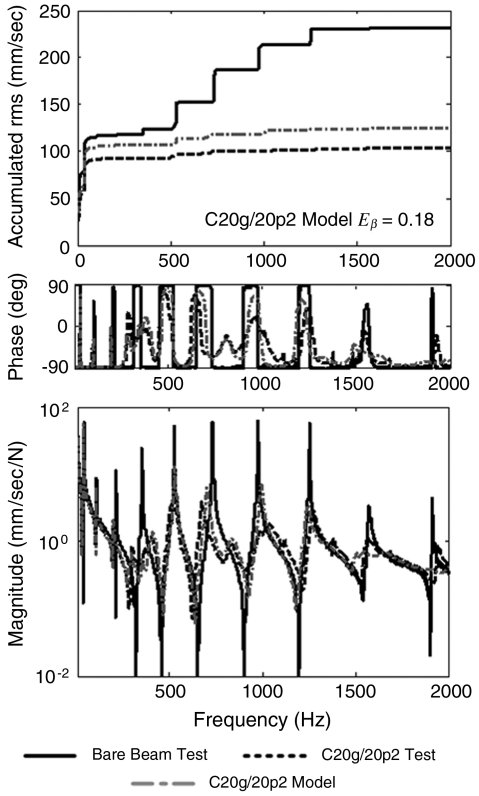

Fig. 27 C20g/20p2 three-segment cable-on-beam FRF and accumulated rms error comparison.

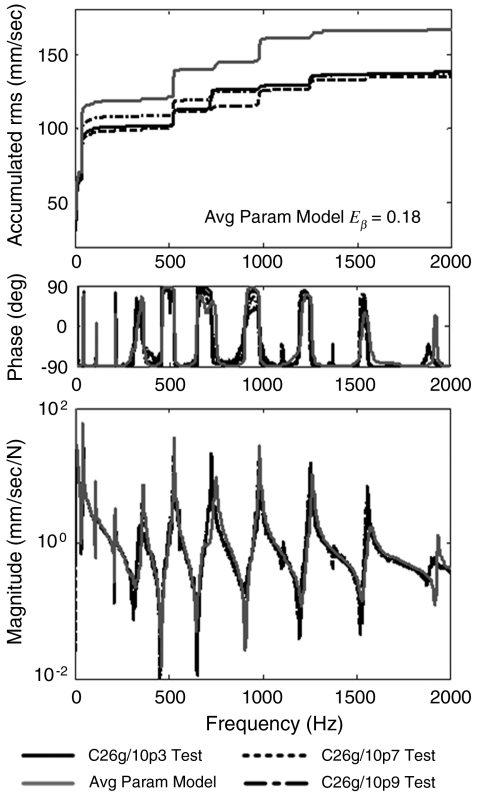

Fig. 28 C26g/10p model and test FRF and accumulated rms error comparison.

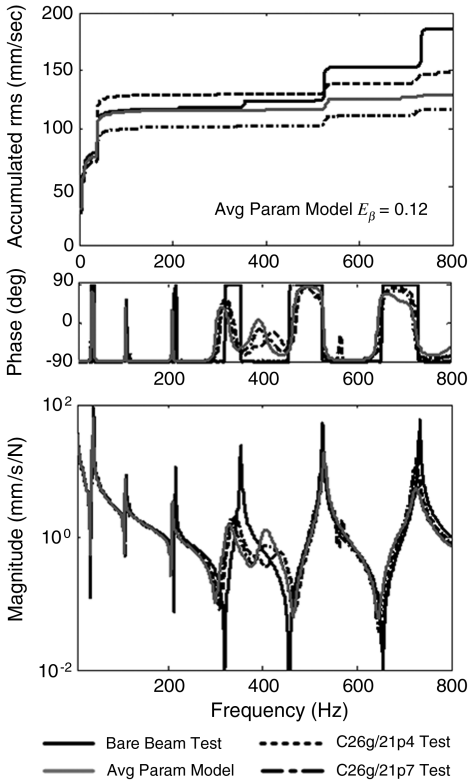

Fig. 29 C26g/21p model and test FRF and accumulated rms error comparison.

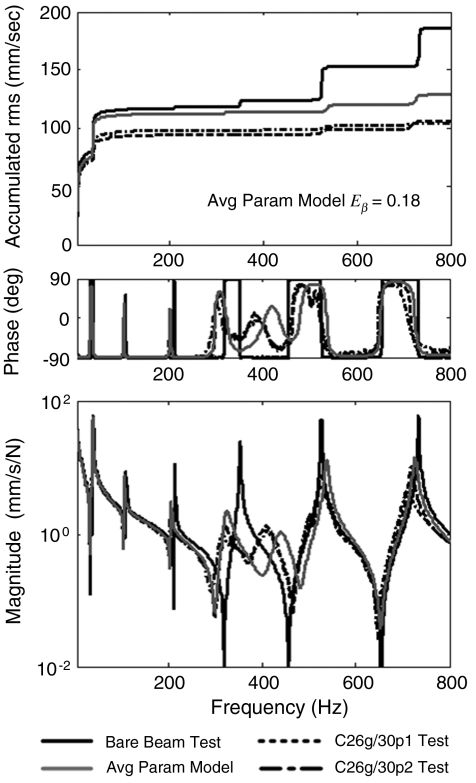

Fig. 31 C26g/30p model and test FRF and accumulated rms error comparison.

Variable Tiedown Spacing

Three cables, 20g/10p3, 20g/20p7, and 26g/21p1, were tested on the host beam, using 203 mm (8 in.) tiedown spacing rather than the 101.6 mm (4 in.) spacing. A typical result is shown in Fig. 32. With the larger tiedown spacing, the interaction between the cable and the host beam seems to be reduced, although this could be an artifact of the different driving point. Nevertheless, the dissipative effect of the cable was observable, and the model predicted the interaction and dissipation of the cable well.

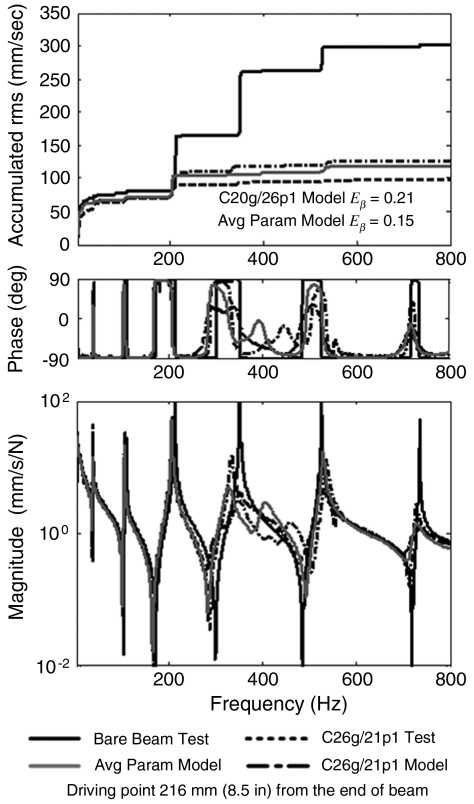

Fig. 30 C26g/21p unstitched cable FRF and accumulated rms error comparison.

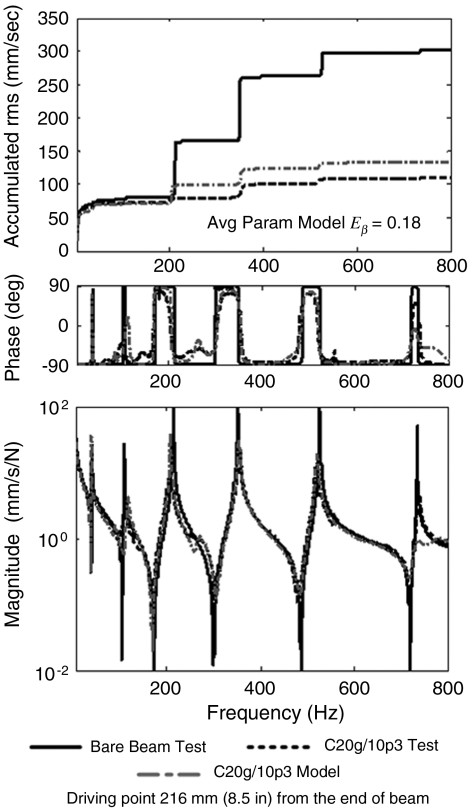

Fig. 32 20g/10p3 cable-on-beam 203 mm tiedown spacing.

Conclusions

This paper identified a neglected area in spacecraft structural dynamics modeling: namely, the interaction between cable wiring harnesses and a host structure. A practical modeling process using industry standard, linear finite element tools was described. FEMs of a cabled beam using empirical cable parameters, tiedown stiffnesses obtained from rod-on-beam tests, and the modeling approach described herein were shown to be valid for all cable families studied. As a result, the finite element modeling approach itself was validated. Furthermore, the cable parameter identification method was validated for use in cable structure models.

The modeling approach introduced cable damping into the model very simply, using an average structural damping value, determined from cable tests, at the element level. This approach carries with it the assumption of constant modal damping in the cables. Often, the damping of the model was slightly low, particularly in the first mode, and influenced the accumulated rms error; however, these damping estimates made the models conservative.

Almost all models that used specimen-specific cable properties were able to better replicate the test FRFs. This implies three things:

1) The cable effects on the structure are sensitive to relatively small changes in the cable properties, and there is benefit to using cable properties for the specific cable used on the cabled structure.

2) The cable properties identified from the cable-only tests are accurate, thereby confirming both the cable parameter identification methodology and its compatibility with the modeling approach described in this paper.

3) The distribution in cable properties across the family must be taken into account when setting expectations on model accuracy when using mean cable family parameters.

All cables affected the response of the host structure. The effects can be divided into two domains. At low frequencies, the cable effect was dominated by mass and stiffness, changing the apparent stiffness; damping was a secondary effect. At higher frequencies, where the cables themselves were resonant, the cable effect was dissipative, increasing the apparent damping in addition to affecting the overall frequency response. The effects of the smallest cables primarily were to introduce additional damping into the structure, with little impact to the modal frequencies. This is consistent with behavior observed in modal tests that involved many accelerometer cables. Larger cables, with mass ratios above 5%, not only increased the damping, they had a significant impact on the modal response of the structure, when the cable modes interacted with the host structure modes. This interaction was always effectively dissipative.

Modeling the cable-to-beam attachment correctly is important for capturing the cables' influences on the host structure. Two important cable-to-beam attachment parameters, tiedown stiffness and the cable neutral axis offset, were identified. The tiedown stiffness was modeled with spring elements, and the cable's discrete attachment to the host structure was modeled with rigid elements. Two methods for estimating tiedown stiffness were discussed. The direct method grossly underpredicted the stiffness. The rod-on-beam configuration was better for estimating the tiedown stiffness. This was not surprising, since this configuration was very close to the test configuration. Not enough data were collected to draw definitive conclusions about how to empirically establish tiedown stiffnesses. A better methodology to estimate tiedown properties is needed. Perhaps experimental determination of the rotational stiffnesses in addition to the axial stiffness would yield a better representation of the tiedown stiffness.

The offset between the cable neutral axis and the host structure neutral axis affected the interaction between the cable and the host structure, more so for stiff cable and rod specimens than more compliant ones. The model should represent the cable-to-host geometric relationship correctly to ensure that the cable stiffness couples with the host structure's stiffness appropriately.

Acknowledgments

The authors would like to acknowledge the support of the U. S. Air Force Office of Scientific Research. The authors are grateful for the contributions made by Greg Mehle and J. Cody Griffee during the research effort. The authors are also indebted to our colleagues with The Aerospace Corporation for their technical reviews of this research. Sandia is a multiprogram laboratory operated by Sandia Corporation, a Lockheed Martin Company, for the U. S. Department of Energy, under contract DE-AC04-94AL85000.

References

[1] Levine, Marie, "Microdynamic Behavior of a Joint Dominated Structure in Orbit," 40th AIAA/ASME/ASCE/AHS/ASC Structures, Structural Dynamics, and Materials Conference and Exhibit, AIAA Paper 1999-1267, April 1999.

[2] "Guidelines for Spacecraft Power and Signal Cabling," ESA CR(P)-1086, 1978.

[3] Costello, G. A., *Theory of Wire Rope*, Springer–Verlag, New York, 1990.

[4] Engberg, R. C., "Umbilical Stiffness Matrix Characterization and Test for Microgravity Science Payloads," 44th AIAA/ASME/ASCE/AHS/ASC Structures, Structural Dynamics, and Materials Conference, AIAA Paper 2003-1873, April 2003.

[5] Griffith, D. T., Carne, T. G., and Paquette, J. A., "Modal Testing for Validation of Blade Models," *Wind Engineering*, Vol. 32, No. 2, 2008, pp. 91–102. doi:10.1260/030952408784815817

[6] Kitis, L., Pilkey, W. D., and Wang, B. P., "Optimal Frequency Response Shaping by Appendant Structures," *Journal of Sound and Vibration*, Vol. 95, No. 2, 1984, pp. 161–175. doi:10.1016/0022-460X(84)90540-6

[7] Ardelean, E. V., et al., "Dynamics of Cable Harnesses on Large Precision Structures," 48th AIAA/ASME/ASCE/AHS/ASC Structures, Structural Dynamics, and Materials Conference, AIAA Paper 2007-2389, April 2007.

[8] Goodding, J. C., Griffee, J. C., and Ardelean, E. V., "Parameter Estimation and Structural Dynamic Modeling of Electrical Cable Harnesses on Precision Structures," 49th AIAA/ASME/ASCE/AHS/ASC Structures, Structural Dynamics, and Materials Conference, AIAA Paper 2008-1852, April 2008.

[9] Robertson, L. M., et al., "Cable Effects on the Dynamics of Large Precision Structures," 48th AIAA/ASME/ASCE/AHS Structures, Structural Dynamics and Materials Conference, AIAA Paper 2007-2389, April 2007.

[10] Goodding, J. C., Babuška, V., Griffith, D. T. , Ingram, B. R., and Robertson, L. M., III, "Study of Free–Free Beam Structural Dynamics Perturbations due to Mounted Cable Harnesses," 48th AIAA/ASME/ASCE/AHS Structures, Structural Dynamics and Materials Conference, AIAA Paper 2007-2390, April 2007.

[11] Han, S. M., Benaroya, H., and Wei, T., "Dynamics of Transversely Vibrating Beams using Four Engineering Theories," *Journal of Sound and Vibration*, Vol. 225, No. 5, 1999, pp. 935–988. doi:10.1006/jsvi.1999.2257

[12] Craig, R. R., and Kurdila, A. J., *Fundamentals of Structural Dynamics*, 2nd ed., Wiley, Hoboken, NJ, 2006.

[13] "MSC.Nastran Basic Dynamics Analysis User's Guide," MSC Software Corp., Santa Ana, CA, 2006.

[14] "Military Specification: Wire, Electrical, Fluoropolymer-Insulated, Copper or Copper Alloy," U. S. Navy MIL-SPEC MIL-W-22759E, Dec. 1990.

[15] "Crimping, Interconnecting Cables, Harnesses, and Wiring," NASA STD 8739.4, 2008.

[16] Goodding, J. C., "Spacecraft Electrical Cable Harness Structural Test and Analysis Methods," International Modal Analysis Conference, Society for Experimental Mechanics, Paper 169, Bethel, CT, 4–7 Feb. 2008.

[17] *Test Requirements for Launch, Upper-Stage and Space Vehicles, Vol. 1: Baselines*, U. S. Dept. of Defense, MIL-HDBK-340A, April 1999.

[18] McConnell, K. G., *Vibration Testing, Theory and Practice*, Wiley, New York, 1995, pp. 391–404.

L. Peterson
Associate Editor